EPJ manuscript No.
(will be inserted by the editor)

Analysis of chaotic non-isothermal solutions of thermomechanical shape memory oscillators

Grzegorz Litak[1,a], Davide Bernardini[2,b], Arkadiusz Syta[1], Giuseppe Rega[2], and Andrzej Rysak[1]

[1] Faculty of Mechanical Engineering, Lublin University of Technology, Nadbystrzycka 36, 20-618 Lublin, Poland
[2] Dipartimento di Ingegneria Strutturale e Geotecnica, Sapienza Universita di Roma, Via Antonio Gramsci 53, 00197, Roma, Italy

Abstract. Shape memory materials exhibit strong thermomechanical coupling, so that temperature variations occur during mechanical loading and unloading. In previous works the nonlinear dynamics of pseudoelastic oscillators subject to an harmonic force has been studied and the possibility of non-regular chaotic responses has been thoroughly documented. Instead of the standard Lyapunov exponent treatment, the statistical 0-1 test based on the asymptotic properties of a Brownian motion chain was successively applied to reveal the chaotic nature of trajectories in the special case in which temperature variations were neglected. In this work, the 0-1 test is applied to fully non-isothermal trajectories. To improve its reliability the test has been applied on the time-histories of maxima and minima of each trajectory, in each component. The obtained results have been validated and confirmed by the corresponding Fourier spectra. Non-regular solutions with different levels of chaoticity have been analyzed and their qualitative difference is reflected by the different values to which the control parameter K asymptotically converge.

1 Introduction

Many materials (metallic alloys, polymers) exhibits the so-called shape memory and pseudoelastic effects and have a broad range of technological applications like, for example: vibration isolation, seismic protection, realization of various types of actuators, switches and sensors [1,2].

Oscillators in which the restoring force is provided by a device with pseudoelastic behavior exhibit complex nonlinear dynamic behavior which may be relevant for several applications and has therefore received considerable interest in the scientific literature in recent years [3–12]. Shape memory materials exhibit a complex thermomechanical behavior due to the solid phase transformations that can be induced by mechanical and thermal inputs. Due to the coupling between mechanical and thermal behavior the temperature may undergo, during mechanical loading, significant

[a] e-mail: g.litak@pollub.pl
[b] e-mail: davide.bernardini@uniroma1.it

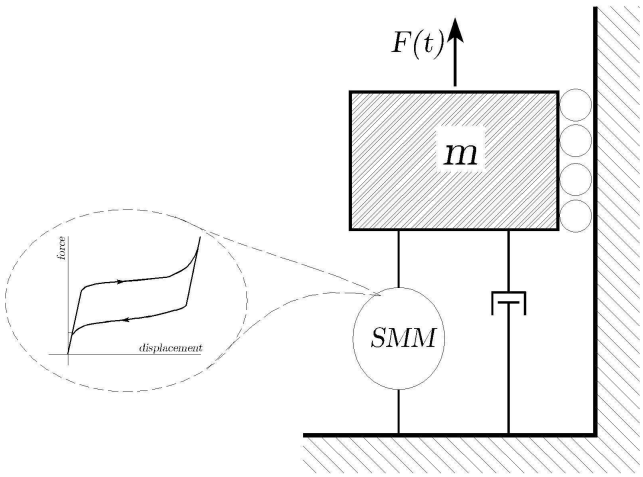

Fig. 1. Schematic picture of a SMD model. SMM denotes a shape memory alloy element with a hysteretic behaviour.

variations that affect the mechanical response. Therefore most of the dynamical applications of such materials should take into account the inherent thermomechanical coupling. Various approaches for the constitutive modeling of shape memory materials are possible [1,2,13]. In this work a fully thermomechanical model introduced and discussed in previous works [5,7] and based on one internal variable representing a phase fraction is used. This type of modeling offers an explicit description of hysteresis, as well as of the prediction of the temperature variations induced by the thermomechanical coupling.

Non-regular chaotic responses in pseudoelastic oscillators has been observed and investigated not only by standard Poincaré maps and Fourier spectra but also with less standard tools like the method of wandering trajectories [8,9]. Due to the increasing number of variables and the system nonsmoothness, the identification of chaotic solutions by the maximal Lyapunov exponent becomes questionable. The present paper is a continuation of the recent papers [8,9] where the test 0-1 is used to distinguish between regular and chaotic solutions [14–18,20]. In [19] the test was validated on a few trajectories computed neglecting the temperature variations. In this work this simplification is removed and fully non-isothermal trajectories are considered. In this case, besides velocity, displacement, and phase fraction, also the temperature is part of the specification of the state and evolves in time. The 0-1 test is applied to all the components of the state and give consistent results. In order to improve its reliability, the method is applied in a modified form in which the analyzed map is obtained by taking maxima and minima of the original time-history. This approach is motivated by an alternative way of description of nonlinear systems proposed by Piccardi and Rinaldi [21] and discussed later by Yang et al. [22]. In their approach they propose to use a peak-to-peak map instead of the standard Poincaré map. This can be useful in cases of higher or fluctuating dimensions of the phase space. Our model with hysteresis is an example of such systems showing solutions with different topologies of attractors.

2 Model and simulations

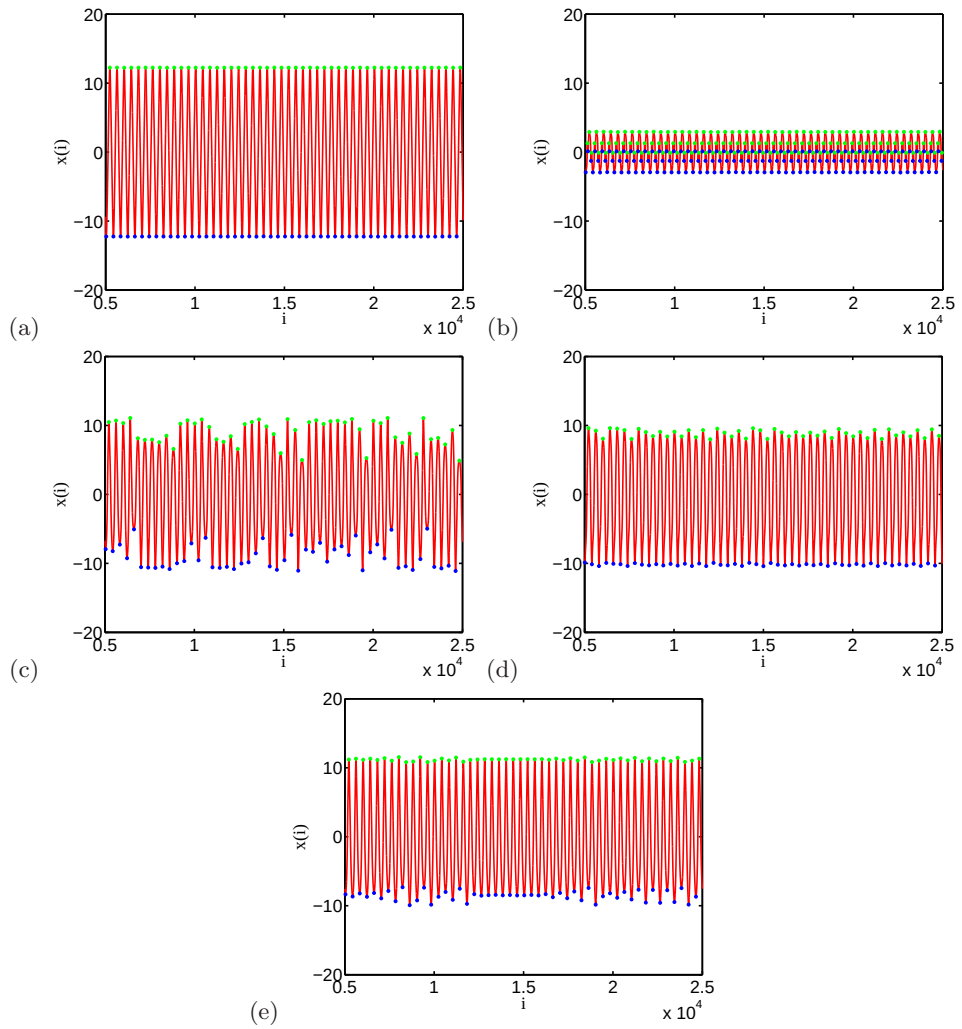

Fig. 2. Time histories of displacement for five different cases specified in Tab. 2. (denoted by a-e). The maxima and minima are denoted by green and blue points, respectively. For discretized time $t_i = i\delta t$, i counts the sampled events with 4000 points per period.

A Shape Memory Oscillator (SMO) is a system composed of a main mass constrained by a suitable assembly of shape memory materials, called Shape Memory Device (SMD), that provides a pseudoelastic restoring force on the main structure (Fig. 1).

SMDs are thermomechanical systems since the solid phase transformations occurring during mechanical loading involve the production/absorption of heat that induces temperature changes that, in turn, significantly affect the mechanical response. As was shown in [5] a suitable constitutive framework for SMO is obtained if at each time t the state of the oscillator is described, besides displacement $x\,(t)$ and velocity

$v(t)$, by an internal variable $\xi(t) \in [0,1]$ that models the internal state of the SMD and by the temperature $\theta(t)$.

In the general modelling framework of [5], the effect of pseudoelastic shape memory devices on mass vibrations is considered within a thermomechanical environment characterized by a harmonic force excitation F and a convective rate of heat exchange Q

$$F = \gamma \cos \alpha t, \quad Q = h(\theta_e - \theta), \tag{1}$$

where γ and α are the excitation amplitude and frequency, θ_e the fixed environment temperature and h the coefficient of convective exchange between the device and the environment (Fig. 1).

Table 1. List of parameters used in the paper

symbol	parameter
t	time
$x(t)$	displacement
x_i, i=1,2,3,...	sampled displacement points
$\overline{x}$, σ_x	average value and standard deviation of displacement
$M(n,c)$	total mean square displacement in new coordinates for n steps corresponding to sampled points
N	length of the sampled points in the displacement time series
$v(t)$	velocity
$p(i)$, $q(i)$	new coordinates obtained by nonlinear transformation
F	harmonic force excitation
γ	excitation amplitude
α	excitation frequency
Q	rate of heat exchange
θ_e	fixed environment temperature
θ	device temperature
h	coefficient of convective exchange between the device and the environment
$\xi \in [0,1]$	internal variable of Martensite fraction (pure Austenite $\xi = 0$, pure Martensite $\xi = 1$)
ξ_0	initial state of ξ variable
λ	denotes the transformation displacement factor maximum displacement that can be obtained by completely transforming the material from Austenite to Martensite
Λ	constitutive function of ξ and θ
sgn(.)	sign function
q_1, q_2, q_3	parameters responsible for modelling of a hysteretic loop, which control the slope of the upper loop plateau, position and slope of the lower loop plateau, respectively
J,Z	thermo-mechanical parameters
K_c and $\tilde{K}$	current (c dependent) parameter of the 0-1 test and its median average over 100 of c values.

Modelling the pseudoelastic restoring force as in Ref. [5,6] and expressing all the quantities in nondimensional form, the dynamics of the system is described by the following equations

$$\begin{aligned} \dot{x} &= v, \\ \dot{v} &= -x + \operatorname{sgn}(x)\,\lambda\xi - \zeta v + F, \end{aligned}$$

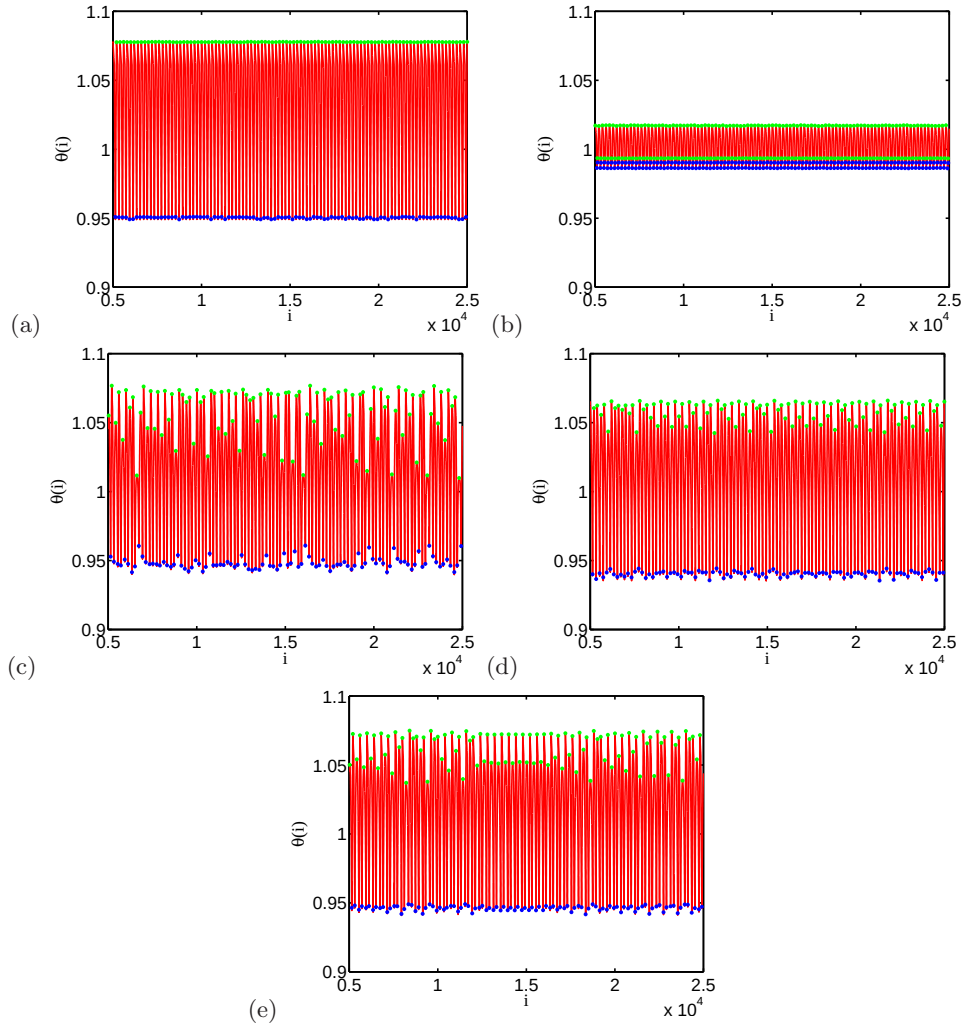

Fig. 3. Time histories of temperature variations for five different cases specified in ab. 2. (denoted by a-e). Note that the temperature oscillations are 2 times faster than the corresponding displacement ones (see the displacement plots in Fig. 2a-e calculated, simultaneously). The maxima and minima are denoted by green and blue points, respectively. For discretized time $t_i = i\delta t$, i counts the sampled events with 4000 points per period.

$$\begin{aligned}\dot{\xi} &= Z\left[\operatorname{sgn}(x)\, v - JQ\right],\\ \dot{\theta} &= ZL\left(\frac{\Lambda}{J\lambda} + \theta\right)\left[\operatorname{sgn}(x)\, v - JQ\right] + Q,\end{aligned} \tag{2}$$

where Λ is a constitutive function of ξ, θ whose explicit expression can be found in [5] and

$$Z = \frac{1}{\lambda + JL\theta + \frac{L}{\lambda}\Lambda + \frac{1}{\lambda}\frac{\partial \Lambda}{\partial \xi}}. \tag{3}$$

All system parameters and symbols used in the paper are presented in Tab. 1

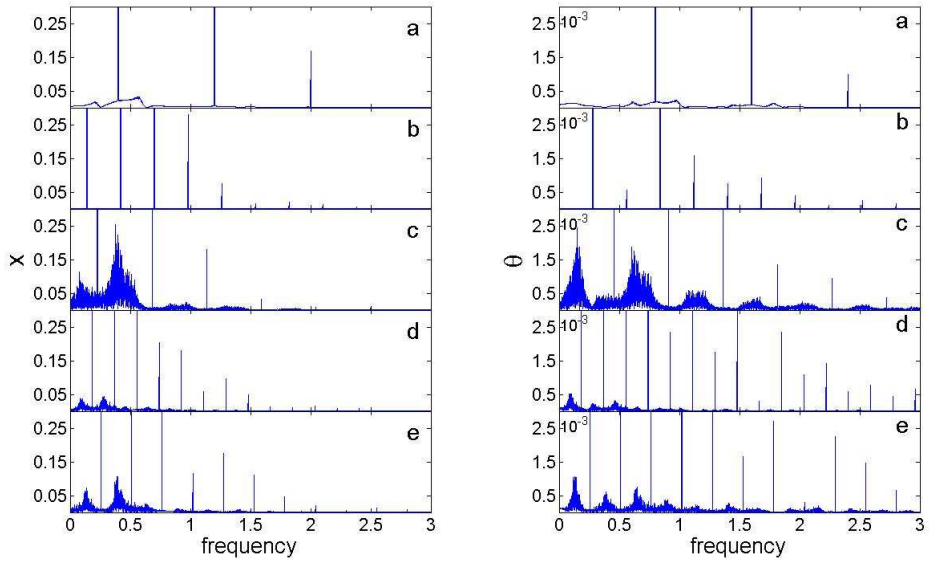

Fig. 4. Fourier spectra for displacement and temperature variations in five examined cases a-e (Tab. 2) calculated simultaneously. The left panel corresponds to displacement, while the right panel to corresponding temperature spectra. Figures a-e in both panels show an enlarged area of the Fourier spectrum for small values of the Fourier amplitudes (the same scale in all subplots of Fig. 4). For graphical reasons the harmonic amplitudes are cut to a fixed value. The actual values of amplitudes of subsequent peaks in Fig. 4a are very different from each other according to the ratios $1 : 0.10 : 0.014$, so that the most important is the first one.

Overall, the constitutive model for the SMD depends on 7 material parameters that can be grouped as follows (see [7] for more details).

Mechanical parameters (q_1, q_2, q_3, λ) that reflect the basic features of the device (type and arrangement of the material) and determine the basic shape of the pseudoelastic loop observed in isothermal conditions. *Thermomechanical parameters* (L, J, h) that determine the features of the temperature variation.

To test the applicability of the 0-1 test to detect chaotic responses the system described by Eqs. 1-3 has been integrated numerically over a time interval of 50000 excitation periods with 4000 points per period under the five combinations of system parameters shown in Tab. 2.

Table 2. Summary of system parameters used in simulations for time series a-b (regular-like response) and c-e (non-regular-like response), respectively.

	model							**excitation**	
Time series	λ	q_1	q_2	q_3	J	L	h	γ	α
(a)	8.125	0.98	1.2	1.017	3.174	0.12	0.08	1.0	0.400
(b)	8.125	0.98	1.2	1.017	3.174	0.12	0.08	1.0	0.140
(c)	8.125	0.98	1.2	1.017	3.174	0.12	0.08	1.0	0.227
(d)	8.125	0.98	1.2	1.017	3.174	0.12	0.08	1.0	0.185
(e)	8.125	0.98	1.2	1.017	3.174	0.12	0.08	1.0	0.255

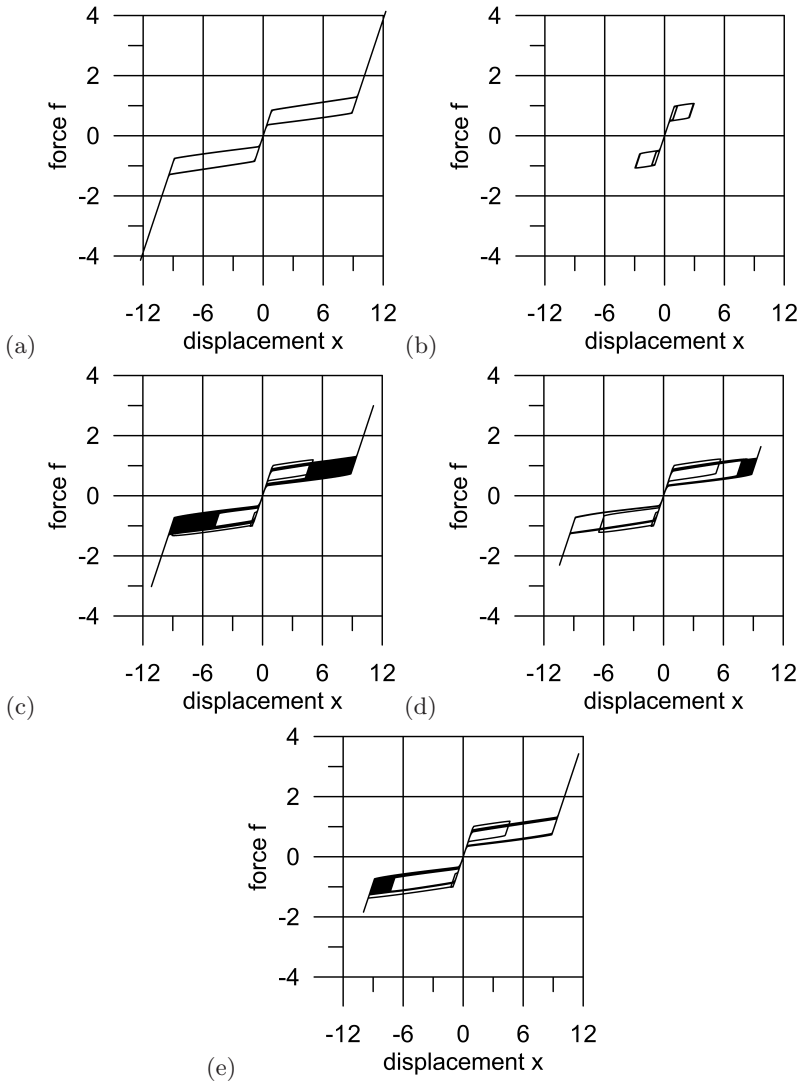

Fig. 5. Hysteretic loop plots (SMD force versus displacement) for the five examined cases. The corresponding systems parameters are listed in Tab. 2.

Such parameter combinations correspond to two regular and three non-regular trajectories. Figures 2 and 5 respectively show the time histories of the displacement and the shape of the hysteretic loops in the force-displacement plane. The two regular trajectories are chosen to be representative of two qualitatively different types of solutions. The first solution, called (a), involves a full hysteresis loop followed by a second elastic branch corresponding to the elastic behavior of the fully transformed material. The second one, called (b), exhibits an hysteretic loop that does not involve the complete phase transformations and thus lacks of the second elastic branch. Similarly, the three non-regular solutions are chosen to be representative of three qualitatively different types of chaotic solutions. The first one, called (c), is a fully developed chaotic solution that involves a rather wide wandering around phase space, symmetric in the

two directions of displacement (like the regular ones). The other two, called (d) and (e) are further chaotic solutions that shows a less extended wandering zone, occurring asymmetrically on the two directions of displacement.

The corresponding time series of temperature are plotted in Fig. 3. Even at a first sight they follow the regularity of displacement (Fig. 2). However their oscillations are 2 times faster than displacement. The Fourier transforms of both displacement and temperature histories are presented in Fig. 4. The first two (a,b) show a discrete-like spectra typical of periodic solutions, with case (b) showing more multiples harmonics of the excitation period. Note that Figs. 2a and 3a represent periodic behaviour with a constant amplitude. The hysteretic phase transition (Martensite -Austenite) is a process that causes nonlinear distortion of the response function and involves harmonic components in the Fourier spectrum. Displacement and temperature change periodically but the shape of periodic functions differ slightly from the harmonic ones. Therefore, as shown in Fig. 4a, there are three main harmonic components, even if one of the three is largely predominant in terms of harmonic amplitude. The other cases (c-e) differ considerably from the previous ones showing the clear bands of frequencies typical of non-regular solutions. Additional information about the solutions is provided by Fig. 5 as described in the previous paragraphs.

3 Test 0-1

To quantify the analysis of regularity of solutions, the 0-1 test has been used for chaos detection [14–16]. This test combines both spectral and statistical properties of the system and can distinguish different types of dynamics of the system by means of the the value attained by the parameter $K \in \{0, 1\}$, defined below. In previous papers [17,20,19], to optimize time of the calculations, the time series was sampled at one quarter of the excitation period or using the concept of average mutual information [23]. In this study a different criterion for sampling is used, namely the histories of local maxima and minima are considered. The peak-to-peak analysis was justified by [21], [22] as an alternative method to the Poincaré series. In the present paper we decided to use maxima and minima map simultaneously to be sensitive to presence and lack of the solution symmetry with respect to the reflection through the point (0,0) (Fig. 5).

Below, one can find the description of the method that, for each set of model parameters, has been applied both to the displacement and temperature time-histories. The discrete points indicated as x_i correspond to the local extrema of the displacement signal and are plotted as coloured points in Fig. 2. Following [19], we change the coordinates from (x_i) to (p, q) with

$$p(n) = \sum_{j=1}^{n} x_j \cos(jc), \quad q(n) = \sum_{j=1}^{n} x_j \sin(jc), \tag{4}$$

where c is a constant, $c \in (0, \pi)$. One can see that (4) is equivalent to the Fourier transform for chosen frequency.

Next, one computes the mean square displacement (MSD) of p and q:

$$MSD(c, j) = \frac{1}{n-j} \sum_{i=1}^{n-j} [p(i+j) - p(i)]^2 + [q(i+j) - q(i)]^2, \tag{5}$$

where $0 \ll j \ll n$ (in practice $n/100 \leq j \leq n/10$). The values of MSD can be bounded in time (for regular dynamics) or unbounded (for chaotic dynamics).

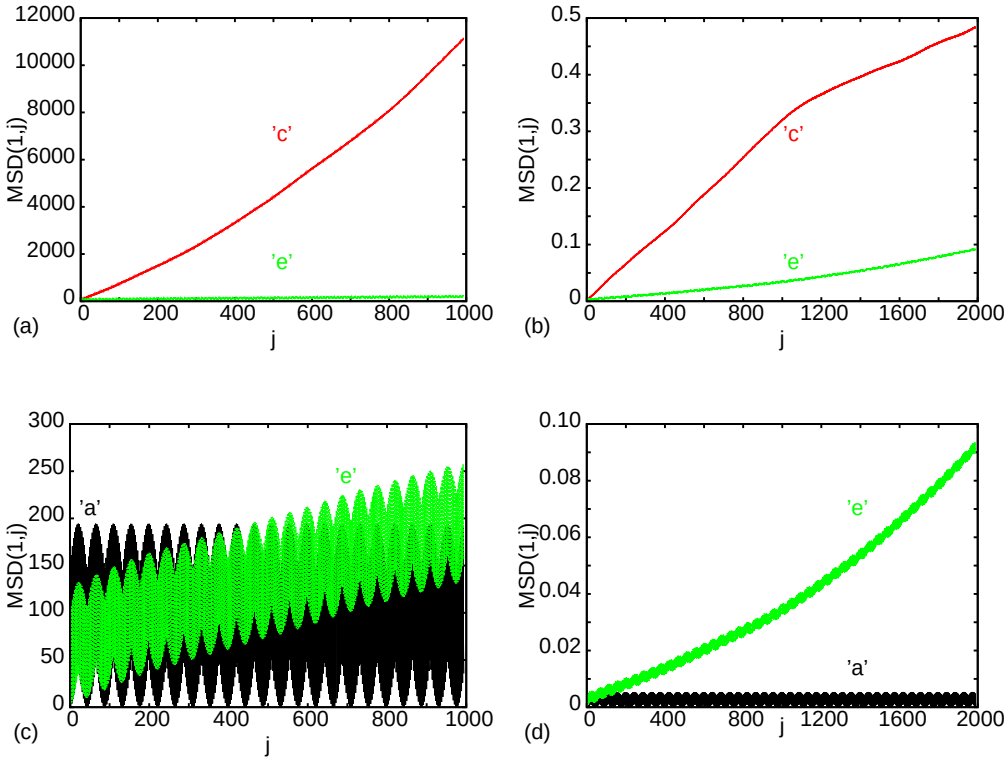

Fig. 6. Mean square displacement calculated for mechanical displacement x (left panel) and temperature θ (right panel), both indicated by the same symbol MSD, as a function of growing time index j in the space (p, q) for $c = 1$. The curves 'a','c', and 'e' correspond to the cases in Tabs. 2 and 3. Note that there is a visible difference between cases related to "strong chaos" and "weak chaos" ('c' and 'e') and "weak chaos" and "regular" ("e" and "a"), respectively (see Tab. 3). Note that $c = 1$ is the specific choice of $c \in (0, \pi)$ which was used in the calculation of $K(c)$ (Eq. 6).

The final quantity K is calculated as an asymptotic growth rate of MSD:

$$K(c) = \frac{Cov[j, MSD]}{\sqrt{Cov[j, j] \cdot Cov[MSD(c, j), MSD(c, j)]}}, \tag{6}$$

where $j = n/100..n/10$, $Cov[j, MSD(c, j)] = E[j - E[j]] \cdot [MSD(c, j) - E[MSD(c, j)]]]$, and the expectation value $E[.]$ estimates the corresponding average.

The value attained by K provides quantitative information about the regularity of the solution, since values close to 0 correspond to regular solutions while bigger values correspond to increasing levels of non-regularity.

The same procedure has been applied not only the displacement but also to the temperature time series $\theta(i)$ (Fig. 3), taking $n = 10000$ for extrema of the displacement and $n = 20000$ for temperature coordinates, due to the different frequency of oscillation of the two variables.

Table 3 shows the values of K obtained for each one of the five trajectories considered on both displacement and temperature histories. Although not reported in the table, results qualitatively similar are obtained if the time histories of the other state variables are considered.

Table 3. K values calculated for extremes of displacement K_x and temperature K_θ.

time series	type of solution	K_x	K_θ
a	regular	-0.001	0.001
b	regular	0.009	0.037
c	"strong" chaos	0.992	0.995
d	"weak" chaos	0.316	0.501
e	"weak" chaos	0.464	0.811

From the results of Tab. 3 it is evident that $K \approx 0$ for solutions (a-b) in both variables x and θ, proving that the trajectories are evidently regular. On the other hand, for the most consolidated symmetric chaotic solution (c), the test yields $K \approx 1$ in both variables which shows a strongly chaotic solution. Interestingly, for the non-symmetric less developed chaotic solutions (d) and (e) the value of K, while being considerably higher than 0 hence proving the non-regularity of the solution, satisfies $K < 1$, namely it is smaller than those of typical chaos. These results seem to suggest that the solutions (d) and (e) are also chaotic but the scale of their attractors is different from that of solution (c). A similar conclusion was obtained in [9] by means of a modified method of wandering trajectories. Note that the particular cases of "regular", "weak chaos", and "strong chaos" differ by the growing MSD increase ratio (Fig. 6).

4 Conclusions

The 0-1 test has been applied to the history of the maxima and minima of the time evolutions of the various components of the response of the thermomechanical pseudoelastic oscillator.

From the obtained results, it turns out that the method is capable to correctly recognize chaotic solutions by analyzing each one of the components. Moreover, it is also capable to detect the difference between chaotic solutions with different strength (Fig. 6). For regular solutions the control parameter K asymptotically tends to 0 while for non-regular solutions it tends to definitely non zero values but with different magnitude that, according to the present simulations, seems to be correlated with different levels of chaoticity.

The estimation of the Lyapunov exponents meets serious problems in embedding dimension determination for non-continuous time-delayed and hysteretic systems, hence nor standard Wolf algorithm with Jacobi matrix [24] nor Kantz algorithm with phase space embedded from time series [25] can be used. In some limited cases, instead of the full phase space, a phase plane subspace could be used for Lyapunov exponent estimation [26]. However it is not clear how to determine the parameter regions of plausible applications for this approximation. In this context, the 0-1 test is very useful because it does not relay on the system dimensionality.

Acknowledgements

The authors gratefully acknowledge the support of the European Union Seventh Framework Programme (FP7/2007-2013), FP7 - REGPOT - 2009 - 1, under grant agreement No. 245479, and Polish National Science Center (GL, AS, AR) under the grant No. 2012/05/B/ST8/00080.

References

1. D.C. Lagoudas (ed.) *Shape memory alloys: modeling and engineering applications* (Springer, Berlin 2008).
2. M. Schwartz (ed.) *Encyclopedia of Smart Materials* vol. 1,2 (Wiley and Sons, New York, 2002).
3. M.A. Savi; P.M.C.L. Pacheco, Int. J. Bif. Chaos **12** (2002) 645-657.
4. L.G. Machado; M.A. Savi; P.M.C.L. Pacheco, **11** (2004) 67-142.
5. D. Bernardini; G. Rega, Math. Computer Model. Dyn. Syst. **11** (2005) 291-314.
6. W. Lacarbonara; D. Bernardini; F. Vestroni, Int. J. Solids Struct. **41** (2004) 1209-1234.
7. D. Bernardini; G. Rega, Int. J. Non-Lin. Mech. **45** (2010) 933-946.
8. D. Bernardini; G. Rega, Int. J. Bif. Chaos **21** (2011) 2769-2782.
9. D. Bernardini; G. Rega, Int. J. Bif. Chaos **21** (2011) 2783-2800.
10. D. Sado; M. Pietrzakowski, Int. J. Non-Lin. Mech. **45** (2010) 859-865.
11. V. Piccirillo; J.M. Balthazar; B.R. Pontes Jr, Nonlinear Dynamics **59** (2010) 733-746.
12. B.C. dos Santos; M.A. Savi, Chaos, Solitons, and Fractals **40** (2009) 197-209.
13. D. Bernardini; T.J. Pence *Mathematical Models for Shape Memory Materials Smart Materials* (CRC press, Taylor and Francis 2009) 20.17-20.28.
14. G.A. Gottwald; I. Melbourne, Proc. R. Soc. Lond. A **460** (2004) 603-611.
15. G.A. Gottwald; I. Melbourne, Physica D **212** (2005) 100-110.
16. I. Falconer; G.A. Gottwald; I. Melbourne; K. Wormnes, SIAM J. App. Dyn. Syst. **6**, 2007, 95–402.
17. G. Litak; A. Syta; M. Wiercigroch, Chaos, Solit. Fract. **40**, 2009, 2095-2101.
18. B. Krese; E. Govekar Nonlinear Dynamics **67** (2012) 2101-2109.
19. D. Bernardini; G. Rega; G. Litak; A. Syta, Proc. IMechE. Part K: J Multi-body Dynamics **227** (2013) 17-22
20. G. Litak; S. Schubert; G. Radons, Nonlinear Dynamics **69** (2012) 1255-1262.
21. C. Piccardi; S. Rinaldi, Int. J. Bifurcat. Chaos **13** (2003) 1579-1586.
22. Y.F. Yang; X.G. Ren; W.Y. Qin, Nonlinear Analysis **68** (2008) 582-590.
23. H. Kantz; T. Schreiber, *Non-linear time series analysis* (Cambridge University Press, Cambridge 1997).
24. A. Wolf; J.B. Swift; H.L. Swinney; J.A. Vastano, Physica D **16** (1985) 285-317.
25. H. Kantz, Physics Letters A **185** (1994) 77-87.
26. L.G. Machado; D.C. Lagoudas; M.A. Savi, Int. J. Solids Struct. **46** (2009) 1269-1286.